IEEE Access
Multidisciplinary | Rapid Review | Open Access Journal

Received September 26, 2019, accepted October 5, 2019, date of publication October 11, 2019, date of current version October 24, 2019.

Digital Object Identifier 10.1109/ACCESS.2019.2947047

A Comprehensive Review of Flux Barriers in Interior Permanent Magnet Synchronous Machines

EHAB SAYED, (Student Member, IEEE), YINYE YANG, (Senior Member, IEEE), BERKER BILGIN, (Senior Member, IEEE), MOHAMED H. BAKR, (Senior Member, IEEE), AND ALI EMADI, (Fellow, IEEE)

Department of Electrical and Computer Engineering, McMaster University, Hamilton, ON L8S 4K1, Canada

Corresponding author: Ehab Sayed (sayede1@mcmaster.ca)

This work was supported in part by the Canada Excellence Research Chairs Program, and in part by the Natural Sciences and Engineering Research Council of Canada (NSERC).

ABSTRACT Interior permanent magnet synchronous machines (IPMSMs) are commonly utilized in many applications where high-torque density and low torque ripple are required. Flux barriers inside the rotor have a great impact on the electromagnetic performance and thus considered as an effective design parameter. This paper provides a comprehensive review of the function and design methodologies of flux barriers in IPMSMs. Both symmetric and asymmetric flux barriers that improve the torque capability and decrease torque ripples are discussed. The paper also investigates different flux barrier designs to reduce the stator and rotor iron losses to enhance the motor efficiency. The optimization of the shape of the flux barriers to mitigate irreversible demagnetization of the rotor magnets is also presented. It is concluded that a good design of flux barriers can significantly improve the motor's electromagnetic performance while reducing the manufacturing costs.

INDEX TERMS Electromagnetic performance, flux barriers, interior permanent magnet synchronous machines, iron losses, torque ripple.

I. INTRODUCTION

Under the scope of cleaner transportation and less tailpipe emissions, vehicle electrification is rapidly reshaping the transportation industry. It also attracts growing customer interests in terms of better drive experience. As one of the key drive components, vehicles demand machines with high performance and high efficiency, which directly determines the vehicle output characteristics. Induction machines [1], [2] are utilized in some electric powertrains. Switched reluctance machines [3]–[6] are the potential candidates to play a critical role in electrification due to the price volatility and supply chain issues with rare-earth permanent magnets. Nowadays, PM machines [7]–[11], specifically interior permanent magnet synchronous machines (IPMSMs), are commonly utilized in electric and hybrid electric vehicles due to their high torque and power densities, high efficiency, and wide speed operation capability.

The associate editor coordinating the review of this manuscript and approving it for publication was Xiaodong Sun.

Motor performance is significantly influenced by its electromagnetic characteristics. Both the stator and rotor designs are critical. Stator geometries are more constrained by the available space, number of phases and winding configurations. The stator parameters play a critical role in the machine performance [12]–[16]. On the rotor side, flux barriers in IPMSM have great impact on the electromagnetic performance. Rotor flux barriers are air voids located in the rotor mainly to prevent the flow of flux between adjacent rotor permanent magnets. Proper design of the flux barriers could significantly improve the torque and power densities. Many articles have studied and presented the benefits of flux barriers. Symmetric or asymmetric designs of flux barriers reduce the torque ripple without applying the typically adopted skewing [17]–[19]. Flux barriers may be designed to reduce stator and rotor iron losses, and improve the motor efficiency. They may also be designed to mitigate irreversible demagnetization of the rotor magnets. However, to the authors' best knowledge, there are no published articles that comprehensively summarize the

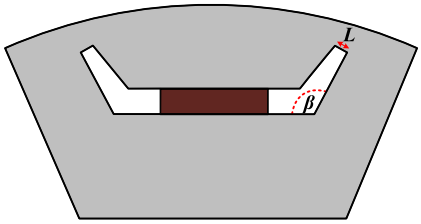

FIGURE 1. Design parameters of the proposed motor [20].

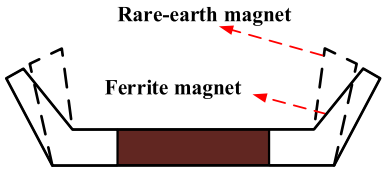

FIGURE 2. Optimal designs in case of ferrite and rare-earth PMs [20].

design aspects of flux barriers and their effects on IPMSM performance.

This paper provides a comprehensive discussion on the approaches and methods of designing rotor flux barriers to improve the electromagnetic performance of IPMSMs. Symmetric and asymmetric designs that improve the torque capability and reduce torque ripples are presented in Sections II and III, respectively. In Section IV, flux barrier designs for iron loss reduction are investigated. Flux barriers designed to mitigate the irreversible demagnetization of rotor magnets are discussed in Section V. Finally, the conclusions are presented in Section VI.

II. SYMMETRIC FLUX BARRIERS

Flux barriers of IPMSMs are commonly designed with symmetry. Flux barriers are typically placed on both ends of the magnets to guide and adjust magnetic field around the rotor poles. One of the main parameters affecting the flux barrier shape is the magnet material. In [20], the effect of the rotor rib shape on the torque ripple has been investigated with different magnet types. A Response surface methodology (RSM) has been utilized to optimize three design parameters (angle β and length L of the flux barriers, shown in Fig. 1, and the magnet remanent flux density).

The objective is to maximize the average torque and minimize the torque ripple with certain upper and lower bounds on the design variables. The residual flux density (remanence) is assumed as 0.5T and 1T for ferrite and rare-earth magnets, respectively. It has been deduced that the average torque is mainly affected by the remanent flux density of the PMs while the other two parameters do not have the same impact. The torque ripple is affected by the distribution of saturated regions within the motor core. Thus, different shapes of flux barriers may be reached for different PM residual flux densities. The optimal designs with each PM material are shown in Fig. 2. Longer flux barrier with smaller angle is obtained when rare-earth PM is utilized. The optimal design in the case

TABLE 1. The optimal values with different PM materials [20].

PM material	Ferrite	Rare-earth
PM residual flux density [T]	0.5	1
Flux-barrier length [mm]	1	3
Flux-barrier angle [deg.]	130	120
Torque [Nm]	3.34	5.52
Torque ripple [Nm]	1.24	1.1

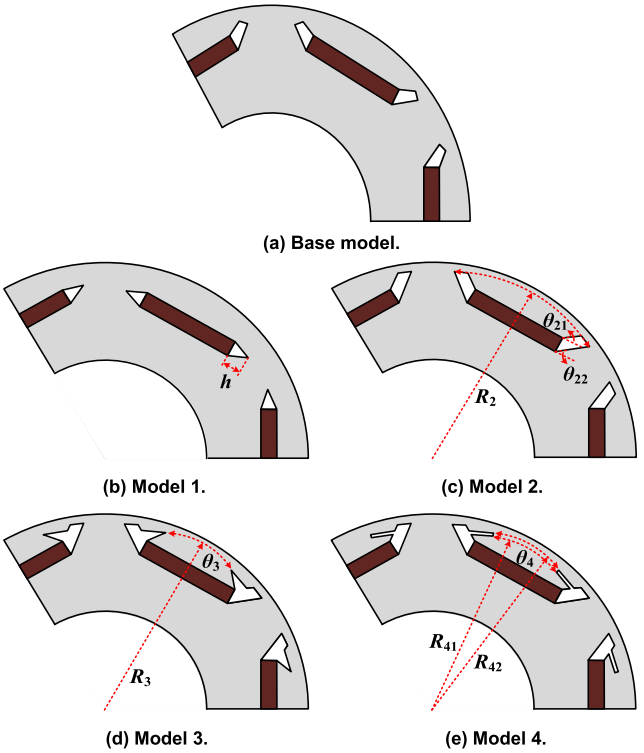

FIGURE 3. (a) Base model, (b) Triangular shape barrier, (c) Trapezoidal shape barrier, (d) Trapezoidal shape barrier with additional triangular layer, (e) Trapezoidal shape barrier with additional straight layer [21].

of ferrite magnet is achieved by a larger flux barrier angle and shorter barrier length. Table 1 presents the optimal values of torque and torque ripple for both designs.

Symmetric flux barriers may have different shapes. In [21], the four different flux barrier shapes shown in Fig. 3 have been studied. Model 1 has triangular shape flux barriers, Model 2 has trapezoidal shape flux barriers, and Models 3 and 4 have the same flux barrier as Model 2 but with an additional layer. The additional layer has triangular shape in Model 3 and straight shape in Model 4.

Taguchi method is used to optimize different design parameters that are designated in Fig. 3 (b)-(e).

h represents the flux barrier height of Model 1. As h increases, the magnetic rib between poles and, hence, magnet leakage flux decreases. R_2 is the radius from the barrier edge to rotor center in Model 2, whereas θ_{21} and θ_{22} represent the barrier upper and lower angles, respectively. As shown in Fig. 3 (d) for Model 3, R_3 and θ_3 represent the radius from the additional flux barrier to the rotor center and the angle

TABLE 2. Torque characteristics of the four models [21].

	Average torque [Nm]	Torque ripple [%]	Cogging torque [Nm]
Base model	206.14	13.4	8.49
Model 1	206.49	7.23	1.16
Model 2	218.23	12.5	5.88
Model 3	223.12	6.47	2.87
Model 4	220.25	8.92	1.58

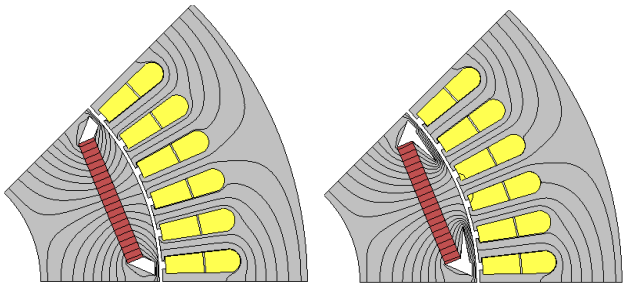

(a) Model 2. (b) Model 3.

FIGURE 4. No-load flux lines of Models 2 and 3 of a 48/8 IPMSM.

between single pole barriers, respectively. For Model 4, R_{41} and R_{42} are the radii from the rotor center to the lower and upper edges of the additional barrier, respectively. θ_4 is the angle between single pole barriers. It was concluded that all the optimized models significantly reduce both the cogging torque and torque ripple. A comparison between the base model, shown in Fig. 3 (a), and optimized models in terms of the average torque, cogging torque, and torque ripple is presented in Table 2.

Model 3 in Fig. 3 (d) has been selected as the final design in [21]. Compared to the base model, it reduces the torque ripple by one half, increases the output torque by 8.2%, and reduces the cogging torque by 66%.

By placing additional flux barriers towards the rotor island in front of the magnets, the additional flux barriers help enhance the d-axis flux density with reduced flux passage area and reduced leakage flux which increase the torque.

Although the additional flux barrier functions like a separate flux barrier layer, it is physically connected to the first layer of flux barrier and, thus, provides a smoother flux path without disturbance in the rotor island in front of the magnets. This also serves to shape the air gap flux density profile. Careful positioning of this additional flux barrier layer will result in more sinusoidal air gap flux density and, hence, reduce the harmonics and the torque ripple.

Following [21] procedure, we applied Models 2 and 3 in Fig. 3 to an IPMSM with 48/8 winding configuration. The no-load flux lines of the two models, obtained by a finite element analysis (FEA) software, are shown in Fig. 4 (a) and (b). A comparison between the no-load airgap flux density of both models is also shown in Fig. 5. It can be noticed that Model 3 has a more sinusoidal flux-density profile with higher amplitude.

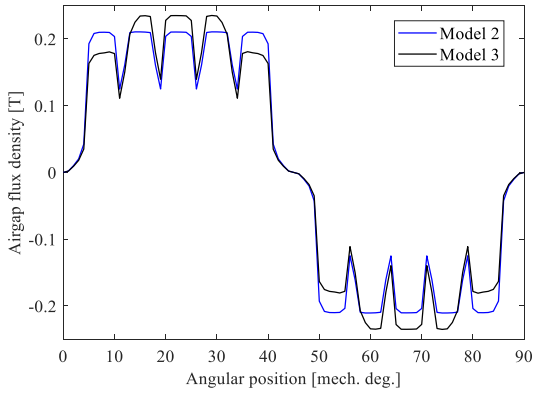

FIGURE 5. No-load airgap flux density of Models 2 and 3 of a 48/8 IPMSM.

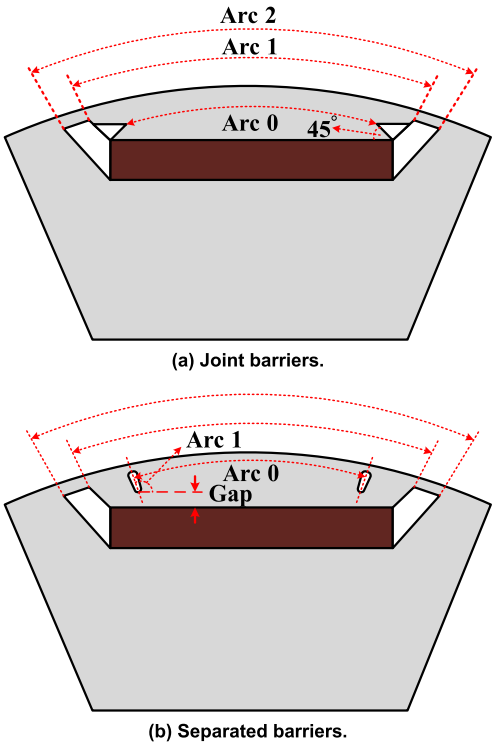

FIGURE 6. Double flux barriers for single-layer IPM motor [22].

Double flux barriers are also utilized in IPMSMs to improve the torque performance. In [22], two rotor configurations with double flux barriers, either joint or separated, have been proposed for single-layer-magnet IPM designs. As shown in Fig. 6, the designs utilize the simple mechanical structure of single magnet layer while utilizing the benefits of double flux barriers to achieve improved torque performance. The IPM rotor flux barrier design is optimized by RSM, which searches the optimized geometry statistically and mathematically to improve the machine performance. Magnet length, flux barrier arc angles, and gap distance between the secondary layer flux barrier and the magnet layer were selected as the optimization parameters to conduct the RSM search. The two-layer flux barrier geometries serve to

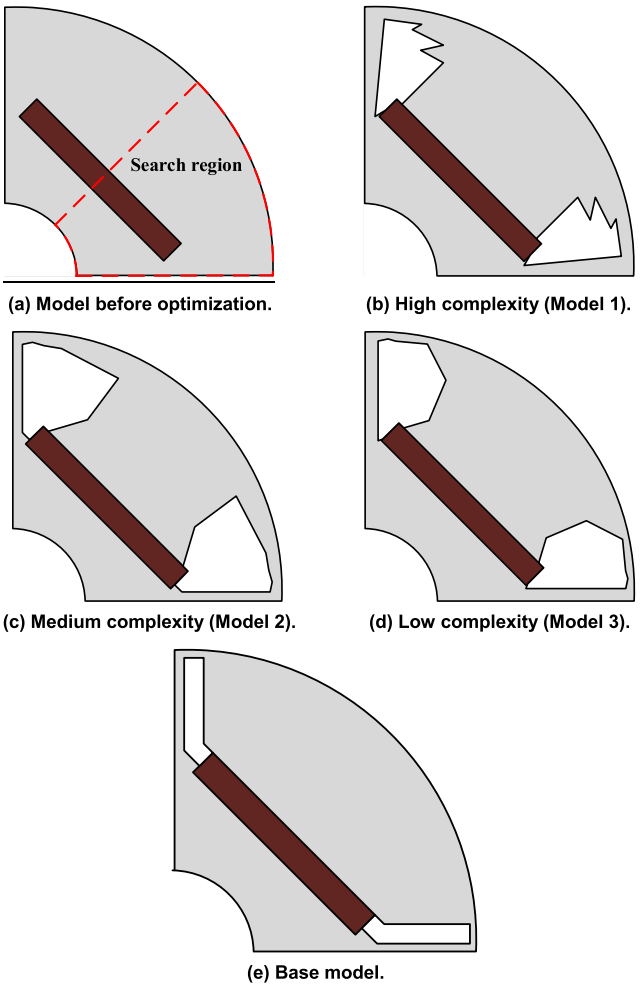

FIGURE 7. Flux barrier design with mathematical optimization [23].

distribute the flux path in the rotor island in front of the single layer magnet and reduce the d-axis inductance and air gap flux density harmonics.

By following the optimization objectives, the search yields low cogging torque and low torque ripple while satisfying rated output torque and low THD harmonics in the back EMF waveform.

It was concluded that, when compared to an optimized conventional single-layer IPM design, the proposed double flux barrier configurations, joint and separated, reduce the torque ripple, by 57.6% and 64.85%, and cogging torque, by 66.7% and 76.7%, respectively.

During the design process of an IPMSM, the shape of the flux barrier should be adjusted along with other rotor parameters. In order to mathematically model and calculate the torque performance using flux barriers, a polygon model method with genetic programming has been used in [23] to shape the flux barrier design.

The optimization objective is selected to be the weighted sum of the average torque, the torque ripple, the cogging torque, and the rotor complexity. The search region, shown in Fig. 7 (a), starts from the shaft diameter to the rotor outer

TABLE 3. Torque characteristics of the three models [23].

	Average torque [Nm]	Torque ripple [%]	Cogging torque [Nm]
Base model	1.83	43.4	0.075
Model 1	2.06	16.4	0.005
Model 2	2.08	19.9	0.006
Model 3	2.12	31.7	0.016

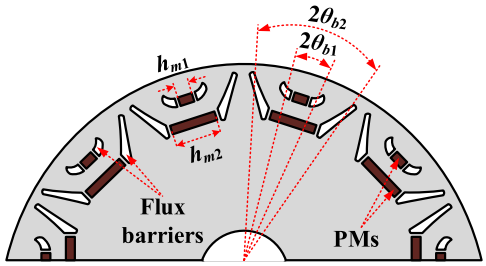

FIGURE 8. Flux barrier optimization using magnetic circuit model [24].

diameter within half of the rotor pole by utilizing the symmetry. By giving different weight factors on flux barrier complexity, three models, shown in Fig. 7 (b)-(d), were obtained to compete with the base model in Fig. 7 (e). Fig. 7 (b) has the most complex shape since the rotor complexity weight is zero. However, it has the lowest torque ripple percentage while keeping a relatively high average output torque.

The other two geometries, Fig. 7 (c) and (d), with less flux barrier complexity also reduce the torque ripple significantly compared to the base model. The average torque, torque ripple, and cogging torque of the three designs are presented in Table 3.

In comparison, all three of the optimized models improve the electromagnetic characteristics. It is obvious that the machine output performance is highly sensitive to the details of the flux barrier geometries. In these three cases, even though the flux barriers share similar location, size, and general shape, their impact on the torque ripple and cogging torque differ significantly.

It is ideal to pursue higher degrees of the flux barrier design complexity to enhance the machine performance. However, this will inevitably result in more demand in computational load during the design phase, as well as higher costs and difficulty in the tooling manufacturing for the lamination punching. The sharp edges in complicated flux barrier geometries are also not practical and they might crack in long-term service. Thus, it is to the engineers' best practice to design flux barriers with moderate complexity that can sufficiently suppress torque ripple and cogging torque, while satisfying reliability and manufacturing requirements.

In [24], a different approach was applied for optimizing flux barriers shown in Fig. 8. An analytical model was used which employs linear slotless stator current sheet [24]. The model considers the stator magnetomotive force (MMF) and the reluctances caused by the flux barriers and magnets.

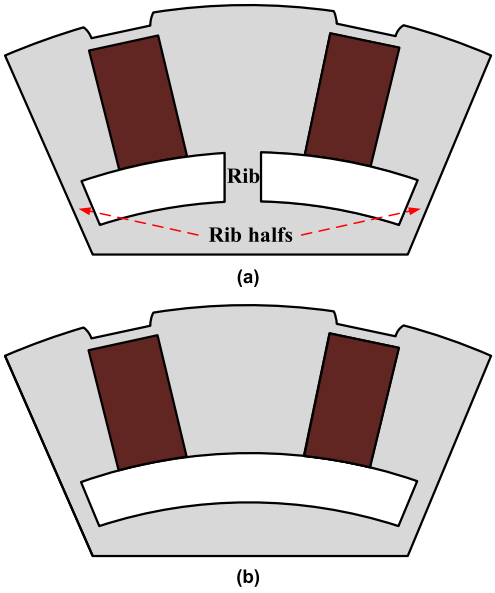

FIGURE 9. Airspace barriers in spoke-type rotor (a) conventional (b) alternate [25].

By varying the geometric parameters of the flux barriers in the magnetic model, the optimized solution can be found analytically. This provides a fast optimization method with high accuracy to reduce the output torque ripple. As shown in Fig. 8, by varying the flux barrier angle, θ_{b1} and θ_{b2}, and the magnet height, h_{m1} and h_{m2}, in the mathematical model, the torque ripple can be minimized while maintaining high output torque. It was shown that the optimized machine provides slightly more torque for the same magnet volume. Moreover, the machine torque ripple is low at both low and high currents.

Flux barriers are also used in spoke-type motors to reduce leakage flux. In conventional flux barrier configurations, shown in Fig. 9 (a), the rib thickness should be small enough to reduce leakage flux but a minimum thickness is required to maintain structural strength, for instance, during high speed operation and during the punching process in manufacturing. This is a tradeoff that cannot be achieved simultaneously in some cases. In [25], an alternative flux barrier for spoke-type motors has been proposed. As shown in Fig. 9 (b), the number of barriers is half that of the poles. This design reduces the leakage flux, even with wider ribs, due to the much lower permeance of the air barrier where the leakage flux flows.

We have run FEA simulations of both designs for a 48/8 IPMSM. The no-load flux lines are shown in Fig. 10. Although the alternate design rib is much wider, the design has less leakage flux.

The torque capability in a spoke-type motor is heavily affected by the leakage flux. Hence, the torque capability in the case of the conventional design in Fig. 9 (a) is sensitive to the rib width, whereas the alternate-barrier design in Fig. 9 (b) shows otherwise.

The torque produced by the alternate-barrier design is reduced from 4.7 to 4.57 Nm, or by 2.7%, when the rib

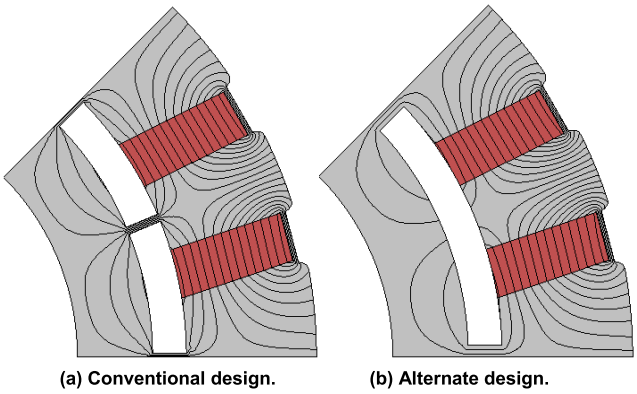

FIGURE 10. No-load flux lines in (a) conventional (b) alternate spoke-type rotor of a 48/8 IPMSM.

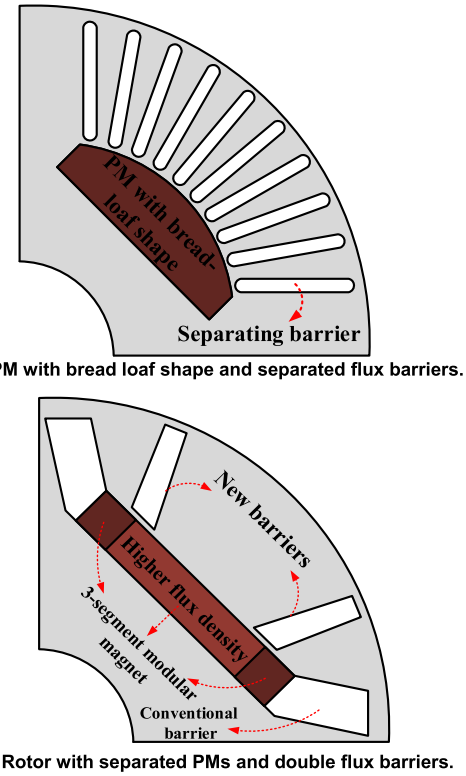

FIGURE 11. Rotor configuration with different types of magnet shapes and flux barriers [26].

width changes from 1.0 to 3.0 mm [25]. This enables designing motors with wider ribs without much effect on the electromagnetic performance. The punching process and, hence, the manufacturing are thus made easier. The maximum mechanical stress in the alternate-design is found to be lower than the yield strength of the silicon steel and the rotor deformation is negligible at high speed.

Symmetric flux barriers are also used in line-start interior permanent magnet machines. Fig. 11 (a) shows a rotor configuration with symmetric flux barriers that divide the rotor island into radial strips [26]. Changing the number of strips and the flux barrier dimensions can shape the air gap flux

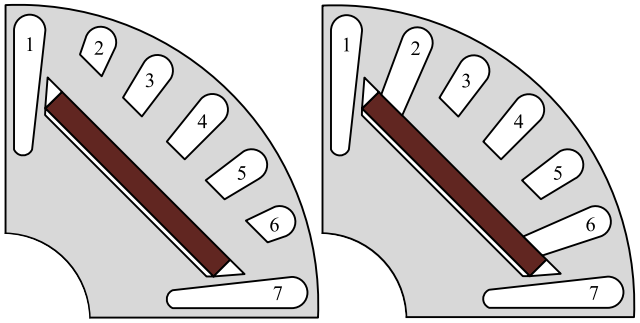

FIGURE 12. Conventional and proposed designs of a LSPM motor [26].

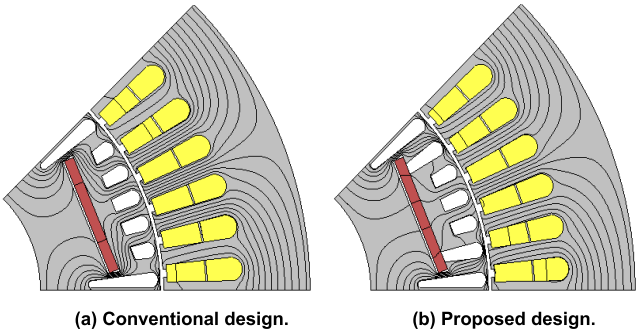

FIGURE 13. Flux lines due to stator direct-axis current excitation in (a) conventional design (b) proposed design of a 48/8 IPMSM.

density, so that it approaches a sinusoidal wave along the airgap. However, too many radial flux barriers prevent the flux flow in the q-axis which reduces the q-axis inductance and, hence, the magnetic saliency ratio and power factor. The design also increases the rotor manufacturing complexity and cost. A configuration is then proposed to achieve better performance as well as manufacturability by reducing the radial flux barriers to two barriers per pole. For this purpose, a three-segment modular pole has been proposed which comprises two different types of PMs such that a PM with higher flux density is located between two PMs with lower flux density as shown in Fig. 11 (b).

The flux barriers help to refine the air gap flux density by reducing the harmonics so that only the fundamental component is intensified and, hence, the air gap flux density becomes more sinusoidal.

A similar flux density distribution can be achieved without utilizing modular magnets. The authors in [26] proposed a design which comprises a simple PM pole with double barriers. For a line-start PM (LSPM) motor, simple PMs may be integrated with the rotor of an existing squirrel-cage induction motor. The non-magnetic rotor aluminum bars serve as flux barriers. The conventional and proposed designs are shown in Fig. 12. Comparing Fig. 12 (a) and (b), the barriers 2 and 6 have been modified in the proposed design to obtain a double-barrier design. This configuration reduces the flux density harmonics and increases the fundamental component. The proposed design in Fig. 12 (b) achieves 11% higher back EMF compared to a conventional rotor with the same amount of magnet volume. Moreover, the barriers 2 and 6 guide the flux produced by stator current to pass through the PM which reduces the d-axis armature reactance. We have run FEA simulations to show that concept for a 48/8 IPMSM. The results are shown in Fig. 13. More flux passes through the magnet in case of extending barriers 2 and 6.

Hence, the proposed configuration has 60% higher ratio of the back EMF to the d-axis armature reactance as compared to that of the conventional configuration [26]. In order to achieve the performance requirements, the proposed machine requires 33% less PM volume compared with the conventional configuration [26].

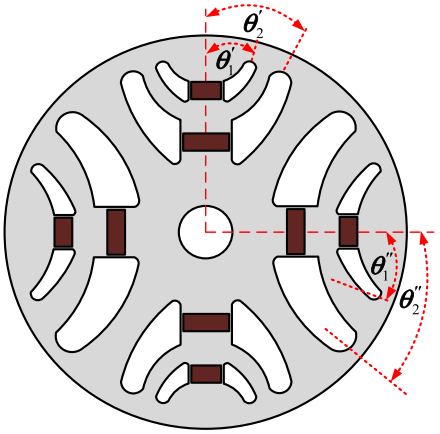

FIGURE 14. Design variables of the Machaon flux barriers [27].

In [27], Machaon type flux barriers have been optimized to increase the average torque and reduce the torque ripple. This flux barrier type is named after Machaon butterfly, which has two large in addition to two small wings [28].

In Machaon structure, as shown in Fig. 14, large flux barriers are located adjacent to small ones. The shape of Machaon flux barrier depends on the winding arrangement, the slot-pole combination of the motor, and the volume of the permanent magnets. A 4-pole 24-slot motor with two different adjacent Machaon flux barriers has been investigated in [27]. TRIBES optimization algorithm based on the motor analytical model is utilized to optimize the angular positions of the flux barrier tips shown in Fig. 14. The shape of the Machaon flux barrier is affected by the winding arrangement. Therefore, in [27], optimizing the shape of Machaon flux barriers with non-chorded and chorded, short-pitched, winding has been analyzed.

When non-chorded winding is utilized, the average torque and torque ripple of the optimized design are 3.74 Nm and 10.98%, respectively. The torque ripple is reduced as compared to previously published Machaon designs [29] with uniform tips ($\theta_1' = \theta_1''$ and $\theta_2' = \theta_2''$). In the case of chorded winding, the torque ripple of the optimized design is further reduced to 8.8%. Moreover, the barrier thickness has been found to have minor effect on both the average torque and

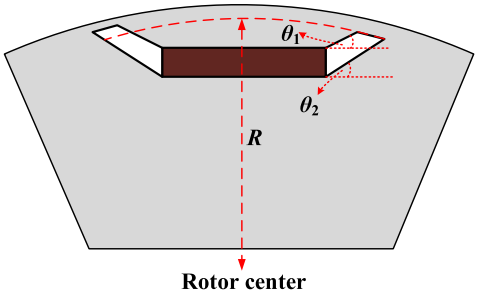

FIGURE 15. Design variables of the motor [30].

torque ripple. However, the number of slots significantly affects the torque ripple since it influences the optimized angles of the flux barriers. The torque ripple decreases as the number of slots increases.

III. ASYMMETRIC FLUX BARRIERS

In symmetric barrier designs, the flux barriers at the sides of each rotor pole are similar. Asymmetric designs may have different geometries or different orientations of flux barriers at both sides. Moreover, flux barriers may exist at only one side of the rotor pole.

In [30], a procedure to reduce the torque ripple and cogging torque of IPMSM has been proposed by utilizing asymmetric flux barriers. An 8-pole 80-kW IPMSM is used in the analysis. The base, symmetric unskewed, motor cogging torque is 3.72 Nm. The motor generates 280.43 Nm at the base speed of 2750 rpm with torque ripple of 17.44%. The torque at the maximum speed of 10000 rpm is 79.96 Nm with 33.68% torque ripple.

Asymmetric flux barriers have been adopted to reduce the torque ripple without skewing. The rotor core is divided axially into two sections with the same lamination geometry. However, one section is flipped 180° and reversely connected to the other. Therefore, the asymmetric flux barriers are aligned axially. The total torque is calculated by summing the torque waveforms of the straight half model and its reverse. The rotor asymmetry affects the magnetic saturation and, thus, the q-axis flux, which reduces the torque ripple. This procedure is different from skewing in that the torque ripples of the two sections are different in magnitude and angle. Unlike skewing, when the torques of both sections are added together, the total torque is increased, whereas the torque ripple is reduced.

Taguchi method has been used to minimize the torque ripple by optimizing three design parameters: the barrier upper and lower angles, θ_1 and θ_2, and the radius R from the bridge to the rotor center as shown in Fig. 15.

The optimized values of θ_1, θ_2, and R are 36°, 36°, and 80.7 mm, respectively. The optimized model has a lower cogging torque of 2.98 Nm, even though this was still higher than a three-step skewed model with 1.5° skew angle.

But, as shown in Table 4, the proposed model has the lowest torque ripple and highest torque. The proposed model also has

TABLE 4. A comparison between the three models at the base speed [30].

Specifications	Base model	3-step skewed model	Asymmetric model
Torque [Nm]	280.43	278.00	282.00
Ripple [%]	17.44	10.06	9.29

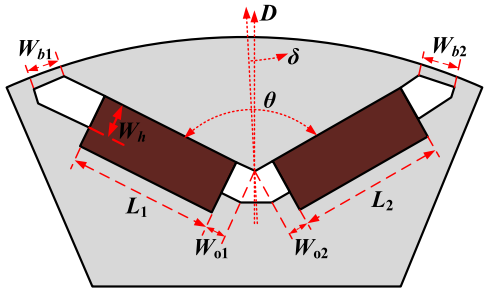

FIGURE 16. Design variables of the V-shaped rotor [31].

23.75% torque ripple at the maximum speed, which is 2.32% lower than that of the skewed model.

In [31], hybrid genetic algorithm-Taguchi procedure is used to produce an asymmetric V-shaped-rotor IPMSM with low cogging torque and torque ripple. The objective is to minimize the cogging torque and torque ripple without or with a slight decrease in the average torque. The torque ripple is required to be less than 6%.

Fig. 16 shows the seven design variables that were utilized to achieve the objectives: asymmetric magnet width ratio L_1/L_2, flux barrier height W_h, left center flux barrier width W_{o1}, right center flux barrier width W_{o2}, left bridge width W_{b1}, right bridge width W_{b2}, and asymmetry angle δ. Three main points should be noted regarding the design variables.

The V-shaped barrier is shifted by an angle δ from the pole pitch centerline D. The two magnets have different widths, L_1 and L_2, and the flux barriers shapes, W_{o1}, W_{o2}, W_{b1}, W_{b2}, are non-uniform.

First, an asymmetric design with the initial specifications is investigated. After that, Taguchi method is utilized to obtain a rough optimized set of the design variables.

The design parameters L_1/L_2, W_{o1}, W_{b1}, and δ are found to be the parameters dominating the torque ripple. These variables are then optimized using genetic algorithm GA.

Four different models have been presented, which are symmetric model S_M, initial asymmetric model I_A_M, Taguchi model T_M, and the hybrid GA-Taguchi model, HGAT_M. A comparison between the average torque T_{avg}, cogging torque T_{Cog}, and torque ripple ΔT of all models is presented in Table 5. The asymmetric designs have slightly lower average torque. However, the torque ripple and cogging torque of these designs have been significantly reduced. The cogging torque and torque ripple of the HGAT_M design are the lowest.

The authors in [32] used assisted barriers in asymmetrical V-shape-rotor IPMSM to make the reluctance and magnet

TABLE 5. A Comparison between the four models [31].

Parameter	S_M	I_A_M	T_M	HGAT_M
W_h [mm]	2.8	3.1	3.1	3.1
L_1/L_2	11.5/11.5	11.8/11.2	11.8/11.2	12.2/10.8
W_{o1} [mm]	1.6	1.6	1.5	1.6
W_{o2} [mm]	1.6	1.6	1.3	1.4
W_{b1}[mm]	2.8	2.7	2.7	2.7
W_{b2} [mm]	2.8	2.7	3.3	3.2
δ [°]	0	4	4	5
T_{avg} [Nm]	21.7617	21.4174	21.4515	21.4242
T_{cog} [Nm]	2.468	1.195	1.097	0.790
ΔT [%]	17.264	9.919	6.597	5.808

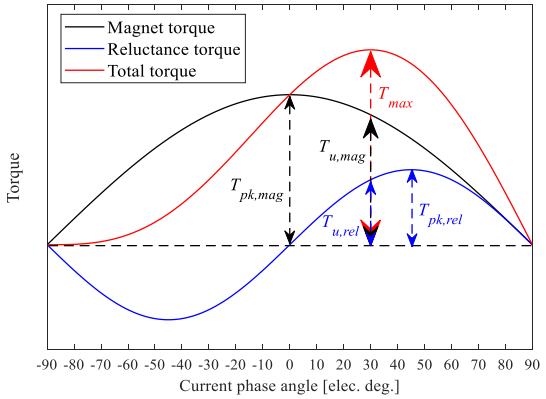

FIGURE 17. Typical torque versus current phase angle characteristics [32].

torques have their maximum at or near the same current excitation angle, which significantly improves the total torque characteristic. These torque components were calculated using the frozen permeability method. As shown in Fig. 17, the utilized magnet and reluctance torques, $T_{u,mag}$ and $T_{u,rel}$, are the torque components that contribute to the maximum value of the total torque T_{max}.

The utilized torques are not coincident with the corresponding peak torques, $T_{pk,mag}$ and $T_{pk,rel}$.

The proposed assisted barriers are located at only one side between adjacent poles. The rotor configuration is shown in Fig. 18. First, the assisted barrier angle γ is chosen as the design variable and an iterative optimization is conducted to maximize the contributions from the magnet and reluctance torques to the maximum value of the total torque. Compared to the original design without assisted barriers, the proposed design increases the maximum average torque by over 35.5% and the efficiency by 6.3% due to the achieved higher torque and lower iron losses. Torque ripple also decreases by 21.7% by using the proposed design configuration.

An optimization process is then conducted to three design variables which are α, γ, and d, shown in Fig. 18, to enhance the motor average torque and efficiency without violating different design constraints on the magnet volume and the upper and lower bounds of the design variables. Compared to

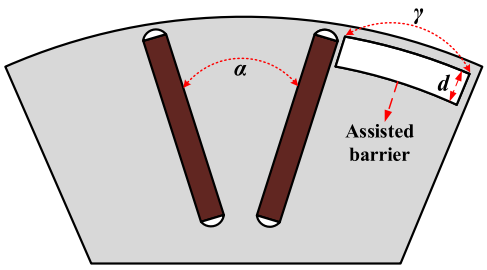

FIGURE 18. Proposed V-type rotor with assisted barriers [32].

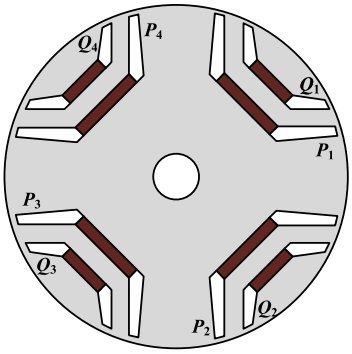

FIGURE 19. Rotor of 4-pole double barrier IPMSM [33].

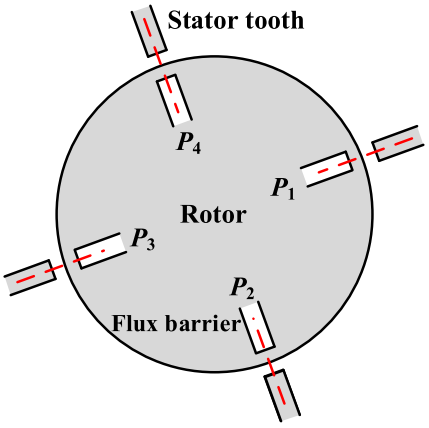

FIGURE 20. Positions of flux barriers edges and stator teeth for symmetrical design [33].

the proposed motor, the optimized motor has 16.6% higher torque, 1.9% higher efficiency, and 18.7% lower torque ripple.

Article [33] proposes another method for asymmetric flux barrier design to reduce the torque ripple without reducing the average torque. The flux barriers are designed such that the relative positions of their outer edges are not aligned with the stator teeth. The rotor is shown in Fig. 19. A 4-pole IPMSM with double barrier layers, labelled P and Q, has been investigated. The relative position of the P layer flux barriers with respect to the stator teeth for a symmetric design is shown in Fig. 20.

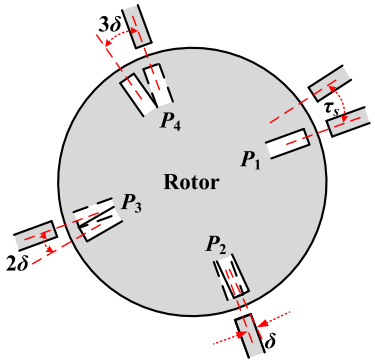

FIGURE 21. Positions of flux barriers edges of P layer and stator teeth for asymmetrical design [33].

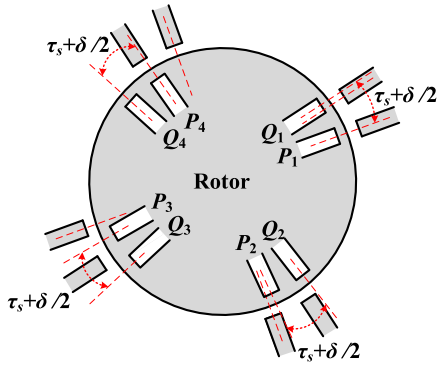

FIGURE 22. Positions of flux barriers edges of P and Q layers for asymmetrical design [33].

In the proposed design, the relative positions between flux barriers' edges and stator teeth are shifted by $n\delta$ relative to the P_1 position, as shown in Fig. 21.

The value of δ depends on the slot pitch τ_s and the number of poles. Moreover, the relative positions of the second flux barrier layer Q are shifted by $\tau_s + \delta/2$ from the corresponding first layer edges. This is shown in Fig. 22. This procedure assures uniform distribution of the relative positions between the flux barriers and stator teeth. The procedure provides significant reduction in the torque ripple. It is applicable to rotors with any number of poles and layers.

One challenge of this design is that it provides limited space for permanent magnets. This restriction can be compensated by using high energy density rare-earth magnets. Another challenge of the design is the increase in the noise and vibration due to rotor asymmetry. This may be overcome by rotating every lamination or every several laminations in the axial direction by 90° or 180°.

Although there is no major difference between the d- and q-axis inductances of the symmetric and the asymmetric designs, there is slight increase in both inductances. The d-axis inductance increase is larger than that of the q-axis inductance. This reduces the reluctance torque. However, the magnet torque increase leads to slightly higher output torque.

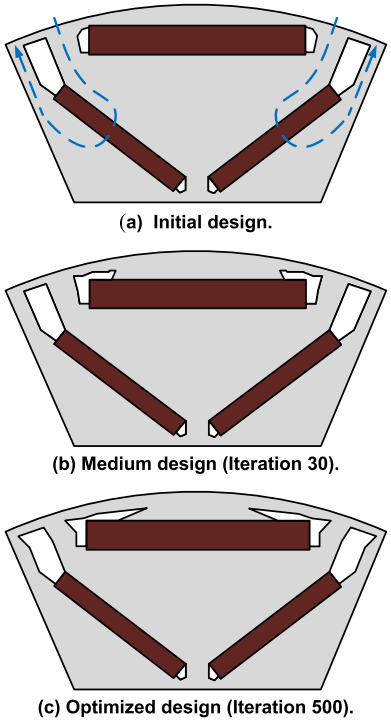

FIGURE 23. Results of the shape optimization process [34].

IV. FLUX BARRIERS FOR IRON LOSS REDUCTION

Apart from improving machine performance, flux barriers also serve an important role to reduce the losses. A good flux barrier design can reduce the machine iron losses and, hence, reduce the internal generated heat. This will improve the machine efficiency as well as improve the thermal loading capacity. In [34], rotor design for a 70-kW 3-phase 8-pole 48-slot IPMSM has been proposed to maximize its average torque and reduce the iron loss. Rosenbrock's method in addition to time-stepping adaptive FEA are used to optimize 20 variables related to the flux barriers and the upper PM dimensions. The optimization process is conducted at peak-torque and field-weakening operating points. The objectives are to minimize the stator iron loss due to PM harmonic MMFs in the field weakening region and to maintain a developed peak torque over 97% of the initial design. The results of the optimization process are shown in Fig. 23. Compared to the initial design, the upper magnet moves away from the rotor periphery and its flux barriers are extended towards the d axis. Thus, the PM flux is concentrated in the island area between the upper magnet and rotor periphery before reaching to the stator.

The authors claim that the optimized design has lower spatial harmonics caused by the PMs, which reduces the stator iron losses. However, this slightly reduces the average torque. Moreover, the maximum mechanical stress of the optimized design, at the maximum speed, is higher than the maximum yield stress including the safety factor of two. Further optimization is conducted to improve the average torque, reduce the core losses, and reduce the rotor mechanical stress. The final optimized design is shown in Fig. 24.

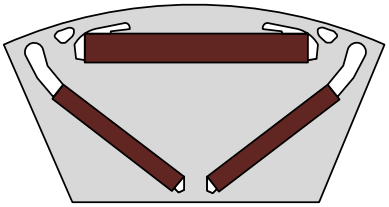

FIGURE 24. Final optimized design [34].

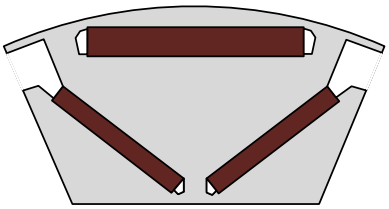

FIGURE 25. Inner flux barriers are joined together [35].

Comparing the electromagnetic performance of the initial and final optimized designs, the following points have been concluded: more than 20% reduction in the iron losses has been achieved. The PM flux linkage is reduced by 9% and there are slight changes in the d-axis and q-axis inductances. The PM torque was reduced, and the reluctance torque was almost the same. Thus, the total torque is reduced by 4% at the peak-torque point. Due to the reduced PM flux linkage, the induced voltage was reduced, and the high-speed continuous torque is improved. Due to the reduction in spatial harmonics, the cogging torque was significantly reduced whereas the torque ripple was slightly reduced. Lower stator core losses due to PMs have been achieved, and there was significant decrease in the iron losses in the field-weakening operating point.

The authors in [34] further optimized the rotor flux barriers in [35] to reduce the rotor losses, including PM eddy-current loss. This prevents the demagnetization due to magnet temperature. The eddy current losses in PMs in a double-layer IPMSM increase due to the slot harmonics. The slot-harmonic flux passes to the rotor through the path between the magnets as shown in Fig. 23 (a). Eddy currents are generated in the inner magnets, which can be reduced by blocking this path.

Based on the initial design shown in Fig. 23 (a), a new flux barrier topology constructed by joining the flux barriers between poles, as shown in Fig. 25, has been presented. This topology reduces the PM eddy current losses but the reluctance torque is reduced as well due to the reduced q-axis inductance.

Based on [35] procedure, we have joined the inner flux barriers of a 48/8 IPMSM. The eddy-current loss density in case of conventional- and joined-barriers designs, at certain rotor position, is shown in Fig. 26 (a) and (b), respectively. The losses have been significantly reduced in case of the joined barriers. However, the reluctance torque dropped from 1pu to 0.81 pu.

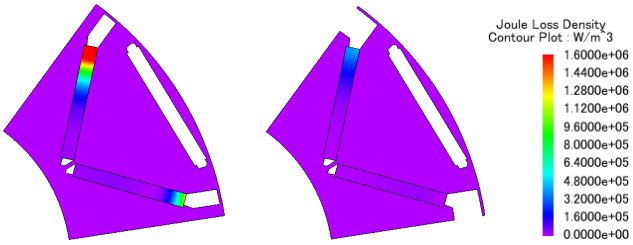

(a) Conventional barriers (b) Joined barriers.

FIGURE 26. Eddy-current loss density in the inner magnets of a 48/8 IPMSM with (a) conventional barriers and (b) joined barriers.

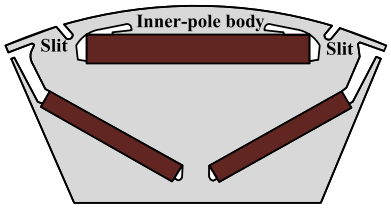

FIGURE 27. Final design with slits and inner-pole bodies [35].

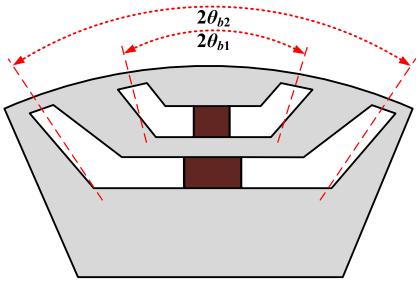

FIGURE 28. The angles of inner and outer flux barriers [36].

In [35], an optimized design is obtained by using Rosenbrock's method along with 2-D electromagnetic and mechanical FEA. The optimization considers the loss reduction, peak torque, and maximum stress on the rotor. The optimized design, shown in Fig. 27, comprises rotor slits besides the inner-pole bodies at the outer magnet. This configuration reduces the losses with 5% reduction in the peak-torque capability. The optimized shape of the flux barriers, together with the inner-pole bodies, reduce the rotor core loss resulting from the slot harmonics. Compared to the initial model, these losses have been decreased by 50%.

For flux barrier design purposes, [36] develops an analytical model to estimate the flux densities in the airgap and stator teeth, and correspondingly calculates the iron losses. The analytical model is then used to develop iron loss factor maps.

These maps are contour plots of the iron loss factor versus the angles of the inner and outer flux barriers, shown in Fig. 28, at a certain magnet thickness, current density, and current angle.

In order to minimize the effect of the magnets on the iron losses, the span angles of the flux barriers, θ_{b1} and θ_{b2}, are selected in the minimum loss region in the maps. The authors studied four designs which all have the same slot-pole configuration. However, the designs have two different sets of flux-barrier span angles. The first set is outside the minimum loss region and the other one is inside that region.

Each set is accompanied with two different magnet heights and, hence, magnet volumes. For the same PM height, the average torque changes slightly at the low speed with changes in the flux barrier angles. For both magnet heights, the first set of flux barrier angles result in higher stator iron loss density regardless of the operating point. This is expected because this set of angles is outside the minimum loss region. For larger PM volume, the iron loss increases due to higher distortion of airgap flux density especially in the field weakening region. However, this increase has been limited by choosing barrier span angles in the minimum loss region.

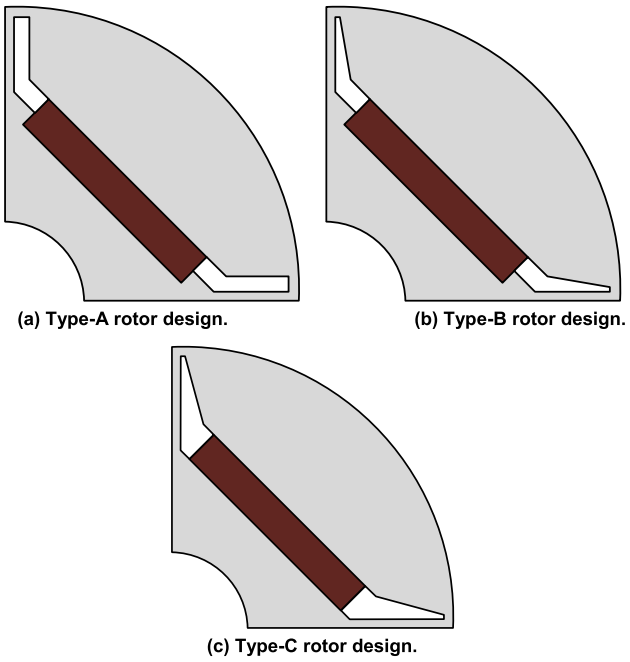

FIGURE 29. Flux barrier shapes and thickness [37].

V. FLUX BARRIERS FOR MITIGATION OF IRREVERSIBLE DEMAGNETIZATION

Magnet demagnetization is a typical concern during IPMSM design. A good flux barrier design can prevent magnet demagnetization in the rotor, improving the machine performance and the maximum machine operating temperature. Either high temperature or high current load can lead to severe magnet demagnetization, while permanent demagnetization could happen if the operating points are beyond the knee point of the magnet *B-H* curve. Flux barriers can be used as a useful tool to prevent irreversible demagnetization. Article [37] investigates the rotor flux barrier shapes and Dy-free rare-earth magnet thicknesses of an IPMSM for both the distributed and concentrated windings.

In this study, three rotor structures have been investigated: (i) rotor with parallel flux barriers (Type-A), (ii) rotor with tapered flux barrier angle (Type-B), and (iii) rotor with tapered flux barrier angle and equal flux barrier and magnet thicknesses (Type-C), as shown in Fig. 29.

It was shown that for both the concentrated and distributed winding models, Type-B and Type-C rotor structures offer superior resistance to demagnetization.

This results from reduced reluctance around the tapered flux barrier angle such that there is more flux passing through the tapered area.

However, this also results that Type-B and Type-C have reduced torque output since there is leakage flux circulating around the tapered area. Compared to Type-B, Type-C is less prone to demagnetization as the armature reaction from the stator MMF surrounding the magnet is lower when the flux barrier and magnet thicknesses are equal.

We have run FEA simulations to investigate the effect of the various structures on the magnet demagnetization of a 48/8 IPMSM. The demagnetization ratio [10] of the magnets with A, B, and C rotor structures is shown in Fig. 30. It shows

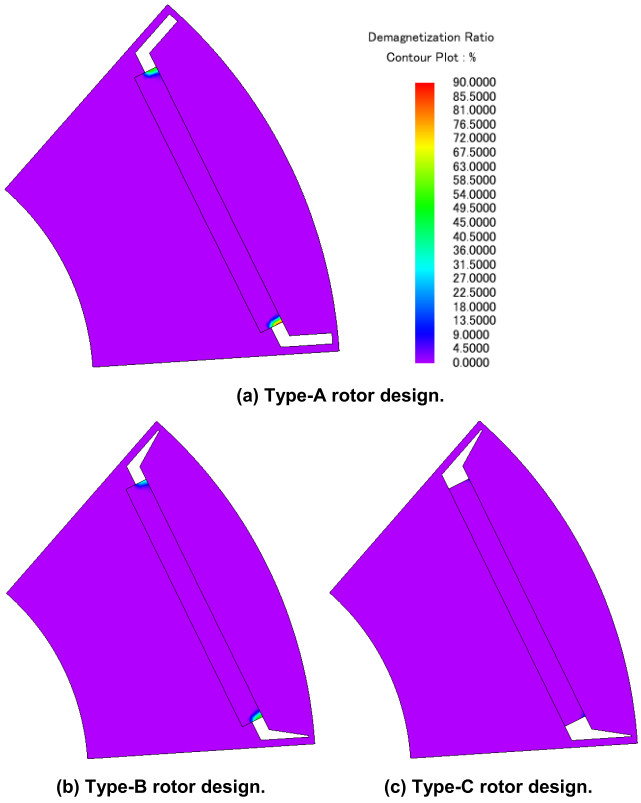

FIGURE 30. Demagnetization ratio of (a) Type-A rotor design (b) Type-B rotor design (c) Type-C rotor design.

that type C is less prone to demagnetization. However, the output torques are 1pu, 0.93pu, and 0.95pu, respectively.

In [38], flux barriers shown in Fig. 31 were implemented to prevent the demagnetization of the rotor magnets. The gap

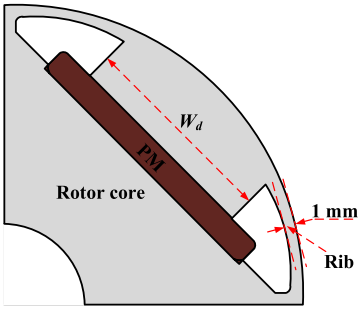

FIGURE 31. Flux barrier design to improve demagnetization endurance in BLDC motor [38].

distance W_d between the two flux barriers under the same pole is selected as the design variable to optimize the demagnetization endurance.

The side rib width between the flux barriers and the rotor periphery is controlled to be fixed at 1mm, considering the trade-off between the rotor mechanical strength and rotor saturation. The gap distance is selected by design of experiments as 13 mm to minimize the cogging torque and torque ripple, and provide sufficient performance to meet the demagnetization requirement. It was concluded that the optimized flux barrier improves the demagnetization resistance under the starting current, or short circuit current, which is the worst case for magnet loading.

VI. CONCLUSION

Flux barriers affect the electromagnetic performance of interior permanent magnet synchronous machines (IPMSMs) significantly. It is one of the most useful tools in motor design to improve output performance and efficiency. This paper provides a comprehensive review for the function and methodologies of the flux barriers in IPMSMs, including the effects of symmetric and asymmetric flux barriers on the motor average torque and torque ripple. Design principles and optimization techniques have also been presented. Symmetric and asymmetric designs can reduce the motor torque ripple and cogging torque while enhancing the torque capability. Flux barriers may also serve an important role to reduce the stator and rotor losses. A good flux barrier design can reduce the machine iron losses and PM eddy-current losses. This reduces the internal generated heat and improves the motor efficiency and thermal loading capacity. A proper flux barrier design can prevent magnet demagnetization, improving the machine performance and the maximum operating temperature. The flux barrier design can also reduce the manufacturing cost and complexity as presented in the alternate-barrier spoke-type IPMSM. However, complex barrier shapes may result in more demand in computational load during the design phase, as well as higher costs and difficulty in tooling manufacturing for lamination punching. A detailed mechanical stress analysis should be conducted since there may be locations with local stresses on the rotor around the barriers. For asymmetric-barrier designs, noise and vibration may increase and the torque performance may not be the same in both rotation directions. These challenges need to be addressed in the design process.

The flux barrier designs presented in this paper can help the electric motor designer to select the proper flux barrier configuration and analysis techniques to improve the performance of their motor design.

ACKNOWLEDGMENT

The authors gratefully acknowledge Powersys Solutions for their support with JMAG software in this research.

REFERENCES

[1] G. Pellegrino, A. Vagati, B. Boazzo, and P. Guglielmi, "Comparison of induction and PM synchronous motor drives for EV application including design examples," *IEEE Trans. Ind. Appl.*, vol. 48, no. 6, pp. 2322–2332, Nov. 2012.

[2] N. Zhao and N. Schofield, "An improved induction machine design procedure for electric vehicle traction," in *Proc. IET Int. Conf. Power Electron., Mach. Drives (PEMD)*, Glasgow, U.K., Apr. 2016, pp. 1–6.

[3] X. Sun, Y. Shen, S. Wang, G. Lei, Z. Yang, and S. Han, "Core losses analysis of a novel 16/10 segmented rotor switched reluctance BSG motor for HEVs using nonlinear lumped parameter equivalent circuit model," *IEEE/ASME Trans. Mechatronics*, vol. 23, no. 2, pp. 747–757, Apr. 2018.

[4] X. D. Xue, K. W. E. Cheng, T. W. Ng, and N. C. Cheung, "Multi-objective optimization design of in-wheel switched reluctance motors in electric vehicles," *IEEE Trans. Ind. Electron.*, vol. 57, no. 9, pp. 2980–2987, Sep. 2010.

[5] X. Sun, K. Diao, G. Lei, Y. Guo, and J. Zhu, "Study on segmented-rotor switched reluctance motors with different rotor pole numbers for BSG system of hybrid electric vehicles," *IEEE Trans. Veh. Technol.*, vol. 68, no. 6, pp. 5537–5547, Jun. 2019.

[6] A. Chiba, K. Kiyota, N. Hoshi, M. Takemoto, and S. Ogasawara, "Development of a rare-earth-free SR motor with high torque density for hybrid vehicles," *IEEE Trans. Energy Convers.*, vol. 30, no. 1, pp. 175–182, Mar. 2015.

[7] X. Sun, C. Hu, J. Zhu, S. Wang, W. Zhou, Z. Yang, G. Lei, K. Li, B. Zhu, and Y. Guo, "MPTC for PMSMs of EVs with multi-motor driven system considering optimal energy allocation," *IEEE Trans. Magn.*, vol. 55, no. 7, Jul. 2019, Art. no. 8104306.

[8] F. Momen, K. Rahman, and Y. Son, "Electrical propulsion system design of chevrolet bolt battery electric vehicle," *IEEE Trans. Ind. Appl.*, vol. 55, no. 1, pp. 376–384, Jan./Feb. 2019.

[9] X. Sun, C. Hu, G. Lei, Y. Guo, and J. Zhu, "State feedback control for a PM hub motor based on grey wolf optimization algorithm," *IEEE Trans. Power Electron.*, to be published.

[10] Y. Yang, S. M. Castano, R. Yang, M. Kasprzak, B. Bilgin, A. Sathyan, H. Dadkhah, and A. Emadi, "Design and comparison of interior permanent magnet motor topologies for traction applications," *IEEE Trans. Transport. Electrific.*, vol. 3, no. 1, pp. 86–97, Oct. 2016.

[11] B. Bilgin, P. Magne, P. Malysz, Y. Yang, V. Pantelic, M. Preindl, A. Korobkine, W. Jiang, M. Lawford, and A. Emadi, "Making the case for electrified transportation," *IEEE Trans. Transport. Electrific.*, vol. 1, no. 1, pp. 4–17, Jun. 2015.

[12] A. Fatemi, D. M. Ionel, N. A. O. Demerdash, and T. W. Nehl, "Optimal design of IPM motors with different cooling systems and winding configurations," *IEEE Trans. Ind. Appl.*, vol. 52, no. 4, pp. 3041–3049, Jul./Aug. 2016.

[13] S. Lim, S. Min, and J.-P. Hong, "Level-set-based optimal stator design of interior permanent-magnet motor for torque ripple reduction using phase-field model," *IEEE Trans. Magn.*, vol. 47, no. 10, pp. 3020–3023, Oct. 2011.

[14] P. Ponomarev, I. Petrov, N. Bianchi, and J. Pyrhönen, "Selection of geometric design variables for fine numerical optimizations of electrical machines," *IEEE Trans. Magn.*, vol. 51, no. 12, Dec. 2015, Art. no. 8114808.

[15] J. S. Choi, K. Izui, S. Nishiwaki, A. Kawamoto, and T. Nomura, "Topology optimization of the stator for minimizing cogging torque of IPM motors," *IEEE Trans. Magn.*, vol. 47, no. 10, pp. 3024–3027, Oct. 2011.

[16] D. G. Dorrell, M. Hsieh, M. Popescu, L. Evans, D. A. Staton, and V. Grout, "A review of the design issues and techniques for radial-flux brushless surface and internal rare-earth permanent-magnet motors," *IEEE Trans. Ind. Electron.*, vol. 58, no. 9, pp. 3741–3757, Sep. 2011.
[17] J. W. Jiang, B. Bilgin, Y. Yang, A. Sathyan, H. Dadkhah, and A. Emadi, "Rotor skew pattern design and optimisation for cogging torque reduction," *IET Electr. Syst. Transp.*, vol. 6, no. 2, pp. 126–135, 2016.
[18] W. Zhao, T. A. Lipo, and B.-I. Kwon, "Torque pulsation minimization in spoke-type interior permanent magnet motors with skewing and sinusoidal permanent magnet configurations," *IEEE Trans. Magn.*, vol. 51, no. 11, Nov. 2015, Art. no. 8110804.
[19] Z. Shi, X. Sun, Y. Cai, Z. Yang, G. Lei, Y. Guo, and J. Zhu, "Torque analysis and dynamic performance improvement of a PMSM for EVs by skew angle optimization," *IEEE Trans. Appl. Supercond.*, vol. 29, no. 2, Mar. 2019, Art. no. 0600305.
[20] Y.-H. Im, S.-I. Hwang, S.-M. Jang, J.-Y. Choi, and J.-H. Choi, "Analysis of torque pulsation considering interior permanent magnet rotor rib shape using response surface methodology," *IEEE Trans. Magn.*, vol. 48, no. 2, pp. 979–982, Feb. 2012.
[21] Z. Pan, K. Yang, and X. Wang, "Optimal design of flux-barrier to improve torque performance of IPMSM for electric spindle," in *Proc. IEEE Int. Conf. Electr. Mach. Syst. (ICEMS)*, Pattaya, Thailand, Oct. 2015, pp. 773–778.
[22] L. Fang, S.-I. Kim, S.-O. Kwon, and J.-P. Hong, "Novel double-barrier rotor designs in interior-PM motor for reducing torque pulsation," *IEEE Trans. Magn.*, vol. 46, no. 6, pp. 2183–2186, Jun. 2010.
[23] K. Ishikawa, W. Kitagawa, and T. Takeshita, "Shape optimization of flux barriers in IPMSM by using polygon model method with GP," in *Proc. IEEE Int. Conf. Electr. Mach. (ICEM)*, Berlin, Germany, Sep. 2014, pp. 1403–1408.
[24] M. Barcaro and N. Bianchi, "Torque ripple reduction in fractional-slot interior PM machines optimizing the flux-barrier geometries," in *Proc. Int. Conf. Electr. Mach.*, Marseille, France, Sep. 2012, pp. 1496–1502.
[25] X. Ge, Z. Q. Zhu, J. Li, and J. Chen, "A spoke-type IPM machine with novel alternate airspace barriers and reduction of unipolar leakage flux by step-staggered rotor," *IEEE Trans. Ind. Appl.*, vol. 52, no. 6, pp. 4789–4797, Nov./Dec. 2016.
[26] E. Sarani and S. Vaez-Zadeh, "Line start permanent magnet motors with double-barrier configuration for magnet conservation and performance improvement," *IET Electr. Power Appl.*, vol. 11, no. 9, pp. 1656–1663, Nov. 2017.
[27] P. Alotto, M. Barcaro, N. Bianchi, and M. Guarnieri, "Optimization of interior PM motors with Machaon rotor flux barriers," *IEEE Trans. Magn.*, vol. 47, no. 5, pp. 958–961, May 2011.
[28] N. Bianchi, S. Bolognani, D. Bon, and M. D. Pre, "Rotor flux-barrier design for torque ripple reduction in synchronous reluctance and PM-assisted synchronous reluctance motors," *IEEE Trans. Ind. Appl.*, vol. 45, no. 3, pp. 921–928, May/Jun. 2009.
[29] A. Vagati, "Synchronous reluctance electrical motor having a low torque-ripple design," U.S. Patent 5 818 140, Oct. 6, 1998.
[30] K.-C. Kim, "A novel method for minimization of cogging torque and torque ripple for interior permanent magnet synchronous motor," *IEEE Trans. Magn.*, vol. 50, no. 2, Feb. 2014, Art. no. 7019604.
[31] W. Ren, Q. Xu, and Q. Li, "Asymmetrical V-shape rotor configuration of an interior permanent magnet machine for improving torque characteristics," *IEEE Trans. Magn.*, vol. 51, no. 11, Nov. 2015, Art. no. 8113704.
[32] W. Zhao, F. Zhao, T. A. Lipo, and B.-I. Kwon, "Optimal design of a novel V-type interior permanent magnet motor with assisted barriers for the improvement of torque characteristics," *IEEE Trans. Magn.*, vol. 50, no. 11, Nov. 2014, Art. no. 8104504.
[33] M. Sanada, K. Hiramoto, S. Morimoto, and Y. Takeda, "Torque ripple improvement for synchronous reluctance motor using an asymmetric flux barrier arrangement," *IEEE Trans. Ind. Appl.*, vol. 40, no. 4, pp. 1076–1082, Jul. 2004.
[34] K. Yamazaki, M. Kumagai, T. Ikemi, and S. Ohki, "A novel rotor design of interior permanent-magnet synchronous motors to cope with both maximum torque and iron-loss reduction," *IEEE Trans. Ind. Appl.*, vol. 49, no. 6, pp. 2478–2486, Nov. 2013.
[35] K. Yamazaki, Y. Kato, T. Ikemi, and S. Ohki, "Reduction of rotor losses in multilayer interior permanent-magnet synchronous motors by introducing novel topology of rotor flux barriers," *IEEE Trans. Ind. Appl.*, vol. 50, no. 5, pp. 3185–3193, Sep./Oct. 2014.
[36] M. Barcaro, N. Bianchi, and F. Magnussen, "Rotor flux-barrier geometry design to reduce stator iron losses in synchronous IPM motors under FW operations," *IEEE Trans. Ind. Appl.*, vol. 46, no. 5, pp. 1950–1958, Sep./Oct. 2010.
[37] K. Imamura, M. Sanada, S. Morimoto, and Y. Inoue, "Improvement of characteristics by flux barrier shape and magnet thickness of IPMSM with Dy-free rare-earth magnet," in *Proc. IEEE Conf. Power Electron. Appl. (EPE)*, Lille, France, Sep. 2013, pp. 1–10.
[38] C.-M. Kim, G.-W. Cho, G.-T. Kim, and H.-G. Shin, "The design of flux barrier for improvement of demagnetization endurance in BLDC Motor," in *Proc. IEEE Int. Conf. Electr. Mach. Syst.*, Busan, South Korea, Oct. 2013, pp. 1198–1201.

EHAB SAYED (S'18) received the B.Sc. degree (Hons.) in electrical engineering from the Shoubra Faculty of Engineering, Benha University, Egypt, in 2010, the M.Sc. degree in electrical engineering, electrical machines and drive systems specialization, in 2016, and the Ph.D. degree in electrical engineering from McMaster University, Ontario, Canada, in 2019. He was a Teaching and Research Assistant with the Shoubra Faculty of Engineering, from 2012 to 2016. He has been with the McMaster Automotive Resource Centre, Ontario, since September 2016. His main research interests include electric drive systems and the design of electric machines for electric and hybrid vehicles and aerospace applications. He serves as a reviewer for the IEEE TRANSACTIONS ON TRANSPORTATION ELECTRIFICATION.

YINYE YANG (S'11–M'14–SM'18) received the B.S. degree in mechanical engineering from Tsinghua University, China, in 2010, the M.S. degree in mechanical engineering from the University of Illinois at Urbana–Champaign (UIUC), USA, in 2010, and the Ph.D. degree in electrical engineering from McMaster University, Canada, in 2014. He joined Magna Powertrain, in 2015, and has been an Adjunct Assistant Professor with McMaster University, since 2016. He is the principal author/coauthor of four patents, eight book chapters, and numerous journals and conference papers. His main research interests include electric machines, electrified powertrain, and integrated mechatronics design. He serves as an Associate Editor for the IEEE TRANSACTIONS ON TRANSPORTATION ELECTRIFICATION and a regular reviewer for multiple journals.

BERKER BILGIN (S'09–M'11–SM'16) received the Ph.D. degree in electrical engineering from the Illinois Institute of Technology, Chicago, IL, USA, in 2011, and the MBA degree from the DeGroote School of Business, McMaster University, Hamilton, ON, Canada, in 2018, where he is currently an Assistant Professor with the Department of Electrical and Computer Engineering (ECE). He is the Co-Founder and the Vice President of Engineering of Enedym Inc., Hamilton, ON, which is a spin-off company of McMaster University. Enedym specializes in electric machines, electric motor drives (EMDs), advanced controls and software, and virtual engineering. He has authored or coauthored 86 journals and conference papers and three book chapters. He is the Principal Inventor/Co-Inventor of ten patents and pending patent applications. His current research interests include electric machines, switched reluctance motor (SRM) drives, acoustic noise and vibration analysis and reduction, and power electronics and EMDs. He is the Lead Editor and the Author of the textbook *SRM Drives: Fundamentals to Applications*.

Dr. Bilgin was the Elected General Chair of the 2016 IEEE Transportation Electrification Conference and Expo (ITEC). He also serves as an Associate Editor for the IEEE TRANSACTIONS ON TRANSPORTATION ELECTRIFICATION.

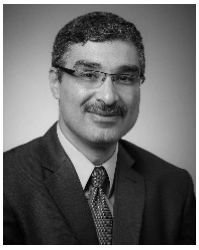

MOHAMED H. BAKR (S'98–M'00–SM'11) received the B.Sc. degree (Hons.) in electronics and communications engineering and the master's degree in engineering mathematics from Cairo University, Egypt, in 1992 and June 1996, respectively, and the Ph.D. degree from the Department of Electrical and Computer Engineering, McMaster University, in September 2000. In 1997, he was a student intern with Optimization Systems Associates (OSA), Inc. From 1998 to 2000, he was a Research Assistant with the Simulation Optimization Systems (SOS) Research Laboratory, McMaster University, Hamilton, Ontario, Canada. In November 2000, he joined the Computational Electromagnetics Research Laboratory (CERL), University of Victoria, Victoria, Canada, as an NSERC Postdoctoral Fellow. He is currently a Professor with the Department of Electrical and Computer Engineering, McMaster University. He is the author/coauthor of over 250 journals and conference papers, two books on the optimization and CAD of high frequency structures, two book chapters on optimization and electromagnetic modeling, and two patents. His research interest include optimization methods, computational electromagnetics, computer-aided design and modeling of power circuits and motors, microwave circuits, THz, photonic devices, nanotechnology, neural network applications, smart analysis of high frequency structures, and efficient optimization using time/frequency domain methods.

Dr. Bakr received a Premier's Research Excellence Award (PREA) from the province of Ontario, Canada, in 2003. He also received an NSERC Discovery Accelerator Supplement (DAS) Award, in 2011. In 2014, he was a co-recipient of Chrysler's Innovation Award for project on novel designs of hybrid cars. Since 2015, he is listed on the Dean's Teaching Honour Roll several times in recognition of his success in utilizing flipped classrooms to teaching engineering courses. He was awarded a Leadership in Teaching and Learning (LTL) Fellowship from the McPherson Institute, McMaster University, in April 2018.

ALI EMADI (S'98–M'00–SM'03–F'13) received the B.S. and M.S. degrees (Hons.) in electrical engineering from the Sharif University of Technology, Tehran, Iran, in 1995 and 1997, respectively, and the Ph.D. degree in electrical engineering from Texas A&M University, College Station, TX, USA, in 2000. He was the Harris Perlstein Endowed Chair Professor of engineering and the Director of the Electric Power and Power Electronics Center and the Grainger Laboratories, Illinois Institute of Technology, Chicago, where he established research and teaching facilities, and courses in power electronics, motor drives, and vehicular power systems. He was the Founder, the Chairman, and the President of Hybrid Electric Vehicle Technologies, Inc. (HEVT), a university spin-off company of Illinois Tech. He was the advisor for the Formula Hybrid Teams at Illinois Tech and McMaster University, which received the GM Best Engineered Hybrid System Award, in 2010, 2013, and 2015 competitions. He is currently the Canada Excellence Research Chair Laureate with McMaster University, Hamilton, Ontario, Canada. He is also the NSERC/FCA Industrial Research Chair in electrified powertrains and a Tier I Canada Research Chair in transportation electrification and smart mobility. He is the principal author/coauthor of over 450 journals and conference papers, and several books, including *Vehicular Electric Power Systems* (2003), *Energy Efficient Electric Motors* (2004), *Uninterruptible Power Supplies and Active Filters* (2004), *Modern Electric, Hybrid Electric, and Fuel Cell Vehicles* (2nd ed, 2009), and *Integrated Power Electronic Converters and Digital Control* (2009). He is also the Editor of the *Handbook of Automotive Power Electronics and Motor Drives* (2005) and *Advanced Electric Drive Vehicles* (2014). He is the Co-Editor of the *Switched Reluctance Motor Drives* (2018). He was a recipient of numerous awards and recognitions. He was the Inaugural General Chair of the 2012 IEEE Transportation Electrification Conference and Expo (ITEC) and has Chaired several IEEE and SAE conferences in the areas of vehicle power and propulsion. He is the founding Editor-in-Chief of the IEEE TRANSACTIONS ON TRANSPORTATION ELECTRIFICATION.